A mathematical framework for forcing turbulence applied to horizontally homogeneous stratified flow

K. J. Rao and S. M. de Bruyn Kops
Department of Mechanical and Industrial Engineering, University of Massachusetts Amherst, Amherst, Massachusetts 01003, USA

(Received 15 December 2010; accepted 19 May 2011; published online 23 June 2011)

It is often desirable to study turbulent flows at steady state even if the flow has no inherent source of turbulence kinetic energy. Doing so requires a forcing schema, and various methods applicable to laboratory experiments or numerical simulations have been studied extensively for turbulence that is isotropic and homogeneous in three dimensions. A review of existing schemata for simulations is used to form a framework for more general forcing methods. In this framework, the problem of developing a forcing method is abstracted into the two problems of (1) prescribing the spectrum of the input power and (2) specifying a force that has the desired characteristics and that adds energy to the flow with the correct spectrum. The framework is used to construct three forcing methods for simulating horizontally homogeneous and isotropic, vertically stratified turbulence. They are implemented in a pseudo-spectral large-eddy simulations and their characteristics are analyzed. The framework is then used to characterize existing laboratory experiments. While no exact analogy can be drawn between forcing in esoteric pseudo-spectral simulations and forcing in physical experiments, there are many similarities. It is suggested that the forcing framework can be applied to predict and systematically test the effects of configuration choices made in the design of simulations and laboratory experiments. © *2011 American Institute of Physics*. [doi:10.1063/1.3599704]

I. INTRODUCTION

Turbulent flows are often approximately statistically stationary because sources of turbulence kinetic energy balance the energy dissipated by the turbulence. Some of the simplest canonical or building block flows useful in research are not inherently stationary. When considering numerical simulations or laboratory experiments to study these simple flows, the question arises as to whether forcing should be applied to make them statistically stationary. In this paper, a framework for developing and analyzing forcing methods is presented and then demonstrated for horizontally homogeneous and isotropic, vertically stratified turbulence in simulations. It is then applied to a series of existing laboratory experiments in isotropic homogeneous turbulence.

Before deciding on a forcing technique, it is useful to consider the merits of forced and unforced flows in order to motivate the development of new forcing approaches. The simplest of all canonical turbulence flows is approximated in the laboratory far downstream of a grid in a wind tunnel, such as in the experiments of Comte-Bellot and Corrsin.[1] Producing a direct numerical simulation of that experiment with the correct energy decay rate requires including in the simulation length scales that are much larger than the integral scale of the turbulence,[2] and even then the simulation results have anomalies that appear to stem from the initialization technique and the finite size of the computational domain.[3] Therefore, despite the use of the best techniques known and significant computational resources, simulations of the most basic of turbulent flows do not necessarily yield results that are as close to the canonical case as one might like. In fact, grid turbulence is inherently an axisymmetric flow that approaches isotropy with time,[4] and so, in the laboratory, forcing via oscillating grids, described by De Silva and Fernando[5] and references therein, and via jets[6–8] have been done to realize flows closer to the ideal.

Forcing flows, either real or simulated, to be statistically stationary through the addition of energy at the largest length scales eliminate the time scale of the energy decay. In simulations, it eliminates the need to devote considerable effort to computing the flow at length scales much larger than the integral scale. In the laboratory, it eliminates the need for a long wind tunnel, to allow isotropy to develop, and the use of Taylor's hypothesis to infer spatial relationships from temporal data. So for some applications, forcing may be a valuable research tool.

In turbulence subject to strong stable stratification, one of the simplest canonical flow configurations is horizontally homogeneous and isotropic with a density gradient in the vertical direction. As with unstratified flows, simulating the "correct" temporal development of the flow might be a distraction from understanding other aspects of the flow physics. In tank experiments, great patience is required to study stratified turbulence because turbulent mixing destroys the stratification, which must be regenerated in order for the experiment series to continue. Riley and de Bruyn Kops[9] ran simulations of a decaying flow inspired by turbulence downstream of a grid in a stratified tank. The results were illuminating, but for a significant portion of the total simulation time, the flow was either strongly influenced by the initial conditions or else had too little energy to be very interesting. Lindborg[10] simulated horizontally homogeneous stratified turbulence forced to stationarity using a stochastic technique.

In that paper, detailed characteristics of the forcing schema were not highly relevant and were omitted, but the study of stratified turbulence forced to be stationary requires a full understanding of the effects of the forcing. In this paper, the forcing of stratified turbulence is used as a test bed of our framework for developing general forcing schemata, and in the process, the characteristics of various approaches to forcing in this flow regime are revealed.

The paper is arranged as follows. In Sec. II, a historical review of forcing is presented with emphasis on simulated unstratified turbulence since most work on forcing techniques has been focused on that flow regime. In Sec. III, the theory is developed using Fourier analysis for random and deterministic forcing of horizontally homogeneous stratified turbulence. The characteristics of the forcing schemata in terms of the temporal accuracy and the rate of convergence to a statistically stationary state are given in Sec. IV. In Sec. V, analogies are drawn between the mathematical formulation and what has been done in the laboratory to create statistically stationary canonical flows. Finally, conclusions are drawn in the last section.

II. BACKGROUND

Historically, the credibility of numerical simulations of fluid flows has depended on favorable comparisons between the simulation results and measurements of physical flows. While acceptance of simulations that are not referenced to specific measurements has increased in recent years, it is nevertheless highly desirable to match simulations to laboratory flows. Doing this for statistically stationary flows outside of boundary layers is a challenge, but some progress has been made in developing laboratory experiments in which turbulence is mechanically forced[5–8,11,12] and in simulations with stochastic real-space forcing.[13,14] The most common approach to applying forcing in simulations of unbounded turbulent flows, however, is to do so in Fourier space. The drawback is that it is easy to create simulated flows that are not realizable in the laboratory, but the mathematical analysis is applicable nevertheless.

A review of the literature on forcing isotropic homogeneous turbulence in spectral simulations and in laboratory experiments reveals interesting parallels. In both fields of research, a forcing method was tried that had desirable and undesirable characteristics, changes were made to reduce the undesirable characteristics, but the changes to the forcing method altered the resulting flows in ways that were hard to isolate. Let us review the history of forcing in simulations to see, with the benefit of hindsight, how a sequence of efforts by many researchers over two decades fit into a systematic framework for forcing.

Kuczaj and Geurts[15] note that forcing techniques can be designed to add constant power or to maintain constant energy in, say, a range of length scales. Forcing can then be implemented via a stochastic approach or a deterministic one. One of the earliest numerical forcing methods sought to maintain the kinetic energy in the flow to be stationary by freezing the amplitude of the velocity in all modes with wave number magnitude in a given range, that is, in a particular "wave number band."[16] This approach requires knowing *a priori* the desired energy in those modes and precludes any effects of motions at small length scales on the dynamics of the large length scales. Chasnov[17] relaxes the latter constraint by requiring that the average energy in a wave number band be held fixed while allowing the energy in each mode to vary. Unfortunately, in the process of converging, schemata of this type suffer from large excursions of the average kinetic energy of the flow.[18,19] Alternative approaches hold constant the average energy in the flow[20,21] and allow the spectrum to evolve to stationarity, which can result in large excursions of the energy at particular wave numbers. This problem in numerical simulations is analogous to the development of secondary flows in laboratory flows, a difference being that in simulations, numerical errors can compound to violate conservation of energy.

To address the problems with slow convergence and large energy fluctuations that are common to many schemata, Overholt and Pope[22] force the flow toward a prescribed energy spectrum over some range of wave numbers but do not require that the target energy spectrum be matched exactly. Instead, a spring-damper analogy is used to construct differential equations for each band of wave numbers, the equations are tuned to be approximately critically damped, and their solutions are used to determine the force magnitudes at each time step. The forcing results in the energy spectrum of the flow optimally approaching the target.

In addition to a mechanism for determining how much power to add to the flow and at what wave number bands, a forcing schema must include a process for distributing the energy across the individual modes that make up a band. In the earliest schemata, the modes were simply frozen. Many later schemata used linear amplification of the existing velocity field.[18,22,23] This approach of adding energy by scaling existing velocities allows the large scales of the flow to evolve in time but it is not clear that the resulting simulation will be statistically stationary, and also large scale anisotropies are frozen.[18] The method of Overholt and Pope uses linear amplification but the amplification factor is dynamically controlled to improve convergence.

Stochastic approaches can also be used to avoid secondary flows in laboratory flows[6] and the related power excursions in simulations. One of the first stochastic forcing methods for simulations is that of Eswaran and Pope.[24] In this approach, random acceleration forces are added when the velocities for the wave number modes being forced are advanced in time. Constraints are imposed so that the resulting velocity field remains non-divergent and that the forces are applied at the desired length scales for the desired duration.

In most of the methods just considered for forcing simulated flows, the kinetic energy is prescribed in one way or another. This is appropriate for flows for which theory is sufficiently developed to guide the selection of the target energy. The theory of stratified turbulence has not advanced to the point of providing such guidance. In fact, only recently, it has been shown that energy input at the large scales of a stratified flow cascades to the small scales.[9,10] Therefore, a class of forcing schemata where power input is prescribed is attractive for simulations of stratified turbulence. In the laboratory, the

power to the forcing mechanism is typically prescribed, but this does not quite equate to prescribe the power transmitted to the flow, as the mathematics in Sec. III reveals.

Ghosal *et al.*[25] developed a non-stochastic, constant-power schema for simulations in which linear amplification is used to add energy to the flow. Stationarity is observed when the dissipation rate fluctuates about the constant power input. Very high energy levels and associated numerical problems can result with schemata of this type because of the time required for the turbulence cascade to develop. As with the constant-energy approaches, the side-effects of linear amplification can be ameliorated by stochastic methods.[26,27] Methods have also been developed in which both the input power and its distribution across several wave number bands are prescribed.[28,29]

A characteristic of many forcing schemata is that they are derived in terms of equations that are continuous in time. Alvelius[30] considers the discrete nature of time in numerical simulations and shows that power input from forcing can result from a force-velocity correlation, as revealed by continuous-time analysis, and a force-force correlation, due to discretizing time. He shows how to make the former zero and how to make the force uncorrelated with itself in time. Lindborg[10] uses a variant of this approach to force the horizontal modes in simulations of stratified turbulence. While laboratory experiments occur in continuous time, there is an analogous effect produced by, e.g., the firing of a jet for a discrete period of time.

III. THEORETICAL DEVELOPMENT

The preceding review reveals that the development of a forcing schema is composed of two subproblems, namely determining how much energy to add at particular length scales and the characteristics of the forces that will inject the prescribed energy distribution. In this section, a framework is developed, using Fourier analysis, that enables the two subproblems to be addressed systematically. To begin, consider a three-dimensional volume of fluid. The evolution equation for the *i*th component of momentum discretized in time is

$$\hat{u}_i^{n+1} = \hat{u}_i^n + \left(\hat{a}_i^n + \hat{b}_i^n\right)\Delta t. \tag{1}$$

The superscript indicates the time step number, the hat signifies that the quantity is in Fourier space, and Δt is the time step. Alvelius[30] demonstrates the importance of considering discrete, rather than continuous, time, and an Euler step is chosen to simplify the analysis. The forces are $\hat{b}_i^n$ from the numerical forcing schema and $\hat{a}_i^n$ from all other sources.

The rate of change of kinetic energy due to the forcing is

$$\frac{\Delta \hat{E}_k}{\Delta t} = \frac{1}{2\Delta t}\left(\hat{u}_i^{n+1}\hat{u}_i^{n+1*} - \hat{u}_i^n\hat{u}_i^{n*}\right) \tag{2}$$

$$= \frac{\Delta t}{2}\hat{b}_i^n\hat{b}_i^{n*} + \frac{1}{2}\left(\hat{u}_i^n\hat{b}_i^{n*} + \hat{u}_i^{n*}\hat{b}_i^n\right), \tag{3}$$

with the asterisk denoting the complex conjugate. The existence of the first term on the right hand side illustrates the importance of considering discrete time since there is no analogous term in the time-continuous evolution equation for energy. In the time-continuous formulation, energy is added to the flow only by the component of the force parallel to and in phase with the velocity, whereas in the discrete formulation, both parallel and orthogonal components of the force add energy. Here, the term "phase" is used in the wave-space and not in the temporal sense.

The Fourier transform of the input power can be divided conceptually into three pieces which we label simply $\hat{P}_1$, $\hat{P}_2$, and $\hat{P}_3$. $\hat{P}_1$ is the power added by the component of the force that is parallel to and in phase with the velocity. $\hat{P}_2$ is the power input due to the component of the force parallel to but exactly out of phase with the velocity so that $Re\{\hat{u}_i^n\hat{b}_i^{n*}\}$ is zero. $\hat{P}_3$ is the power due to the component of the force perpendicular to the velocity. Relating $\hat{P}_1$, $\hat{P}_2$, and $\hat{P}_3$ to $\hat{b}_i^{n*}$ and $\hat{u}_i^{n*}$ is deferred until Sec. III A. For now, our interest is in the concept that

$$\frac{\Delta \hat{E}_k}{\Delta t} = \hat{P} = \hat{P}_1 + \hat{P}_2 + \hat{P}_3. \tag{4}$$

Thus far, the framework for forcing is general. Implementing a specific forcing schema requires three addition steps, which are detailed in Secs. III A–III C for horizontally homogeneous and isotropic forcing. The first step is to impose constraints on the force direction and phase. This determines the contributions of $\hat{P}_1$, $\hat{P}_2$, and $\hat{P}_3$ to the forcing spectrum. In most schemata, the only constraint is that the force does not cause the velocity field to be divergent, but Alvelius[30] shows how to choose the force so that it is uncorrelated with the velocity field. Second, the left hand side (LHS) of Eq. (4) must be chosen. In many schemata, Eq. (4) is averaged over wave number bands so that it is in terms of discrete power spectra. The LHS is then the spectrum of the input power, hereafter referred to as the "forcing spectrum." For instance, in the schema of Overholt and Pope[22] the forcing spectrum is determined by solving differential equations for each wave number band to optimally converge the simulation to a model power spectrum. In the schema of Alvelius,[30] the forcing spectrum is a Gaussian, centered at a specific wave number and invariant in time. The third step in developing a forcing schema is to combine the previous two steps into a practical algorithm.

A. Constructing a horizontally homogeneous and isotropic force

To develop a forcing schema that is horizontally homogeneous and isotropic, consider a horizontal force, $\hat{h}_i(\kappa)$, invariant in the vertical direction, that is, $\hat{h}_i \equiv 0$ if $\kappa_3 \neq 0$. Here, $\boldsymbol{\kappa} = (\kappa_1, \kappa_2, \kappa_3)$ is the wave number vector. This force expressed in terms of phase and magnitude is

$$\hat{h}_i(\kappa_1, \kappa_2, 0) = \left|\hat{h}_i(\kappa_1, \kappa_2, 0,)\right| e^{i\theta_h} e_i, \tag{5}$$

with e_i the unit vector defining the direction, $|\ |$ denoting the magnitude of a complex number, and θ_h the phase. It can be shown that, if the horizontally homogeneous isotropic force is non-divergent, then the two horizontal components of the force have the same phase, θ_h. The force is applied for the

duration of time step n, but the superscript indicating the time step number is omitted to avoid cumbersome notation.

The complex velocity in the plane $\kappa_3 = 0$ can be expressed similarly as

$$\hat{u}_i(\kappa_1, \kappa_2, 0) = |\hat{u}_i(\kappa_1, \kappa_2, 0)| e^{i\theta_u} e_i, \tag{6}$$

where θ_u is the phase of velocity. From continuity, $\kappa_1 e_1 + \kappa_2 e_2 = 0$ so that $e_i = (-\kappa_2, \kappa_1)/\kappa_h$, where $\kappa_h = \left(\kappa_1^2 + \kappa_2^2\right)^{1/2}$. The constraint that the force does not cause divergence in the velocity field requires that the force and velocity be parallel and so e_i in Eqs. (5) and (6) must be the same vector.

Next, so that the force is horizontally homogeneous, denote an integral over a circle of radius κ_h by $\oint (\,) d\mathcal{S}(\kappa_h)$, and define

$$U(\kappa_h) = \oint (|\hat{u}_i(\kappa_1, \kappa_2, 0)|) d\mathcal{S}(\kappa_h),$$
$$H(\kappa_h) = \oint (|\hat{h}_i(\kappa_1, \kappa_2, 0)|) d\mathcal{S}(\kappa_h),$$

and

$$P(\kappa_h) = \oint \hat{P}(\kappa_1, \kappa_2, 0) d\mathcal{S}(\kappa_h).$$

The latter is simply the forcing spectrum. In terms of the velocity and the horizontal force spectra,

$$\begin{aligned} P(\kappa_h) &= \frac{\Delta t}{2} H^2(\kappa_h) + H(\kappa_h) U(\kappa_h) \frac{\left(e^{i(\theta_h - \theta_u)} + e^{-i(\theta_h - \theta_u)}\right)}{2} \\ &= \frac{\Delta t}{2} H^2(\kappa_h) + H(\kappa_h) U(\kappa_h) \cos(\theta_h - \theta_u), \end{aligned} \tag{7}$$

which is a quadratic equation in $H(\kappa_h)$. Given a forcing spectrum, $P(\kappa_h)$, $H(\kappa_h)$ is now defined. Furthermore, we have arrived at the comforting result that for the force, h_i, to be real, $P(\kappa_h)$ must be non-negative (c.f. Sec. III B). The first term on the RHS of Eq. (7) corresponds to the power input due to the spatial force-force correlation at a given discrete time-step. That is, it is the horizontal spectrum corresponding to $\hat{P}_1$, which arises from the discretization of time in a simulation. The second term is due to the force-velocity correlation and corresponds to $\hat{P}_2$. A term corresponding to $\hat{P}_3$ cannot occur in this forcing schema because of the requirement that in 2D the force be parallel to the velocity in order to avoid forcing the flow to be divergent.

Equation (7) provides the magnitude of the force that will add to the flow power with spectrum $P(\kappa_h)$. It remains to select the phase of the force. In general, θ_h is a free parameter that can be selected, e.g., stochastically. In this research, the limiting cases of the force and velocity being exactly in phase or out of phase are considered and their magnitudes are denoted $F(\kappa_h)$ and $G(\kappa_h)$ that satisfy the equations

$$P(\kappa_h) = \frac{\Delta t}{2} F^2(\kappa_h) + F(\kappa_h) U(\kappa_h), \tag{8}$$

$$P(\kappa_h) = \frac{\Delta t}{2} G^2(\kappa_h). \tag{9}$$

The force magnitudes have been defined as functions of κ_h. The force can be a function of the local wave number components, κ_1 and κ_2, and so there remains a free parameter in the description of the force, namely the distribution of the force among all the nodes with horizontal wave number magnitude $\kappa_h - \Delta\kappa_h \leq \kappa_h < \kappa_h + \Delta\kappa_h$, where $\Delta\kappa_h$ defines the size of a wave number band. In this paper, entirely different approaches are used for choosing this free parameter for the in-phase force than for the out-of-phase force. For the former, it is reasoned that force is applied by amplifying the velocity magnitude and so is inherently distributed across the wave number band. It could be distributed a different way, but a physical justification for doing so is not clear and we choose not to. Therefore,

$$\hat{f}_i(\kappa_1, \kappa_2, 0) = F(\kappa_h) e^{i\theta_u} e_i. \tag{10}$$

The out-of-phase force arises entirely from the discretization of time and, therefore, it has no physical analog. It is inherently uncorrelated with the velocity. As shown by Alvelius, it can also be made uncorrelated with itself in time if it is stochastically distributed among the modes in the wave number band. To do this, $G(\kappa_h)$ is replaced by $A(\kappa_h)B(\kappa_1, \kappa_2)$ with $B(\kappa_1, \kappa_2)$ a real random variable uniform in $[0 \ldots 1]$ and $A(\kappa_h)$ defined by

$$A^2(\kappa_h) = \frac{G^2(\kappa_h)}{\oint B^2(\kappa_1, \kappa_2) d\mathcal{S}(\kappa_h)}. \tag{11}$$

Thus, the out-of-phase force is

$$\hat{g}_i(\kappa_1, \kappa_2, 0) = A(\kappa_h) B(\kappa_1, \kappa_2) e^{i\theta_u + \pi/2} e_i. \tag{12}$$

B. Selection of forcing spectrum

In Sec. III A, it is shown how to construct forces that will yield a given forcing spectrum, $P(\kappa_h, t)$. Here, the dependence of the forcing spectrum on time is explicitly shown. As reviewed in Sec. II, quite a few approaches have been used in the past to prescribe the forcing spectrum for turbulence that is homogeneous and isotropic in all three directions. Here two methods are presented for specifying $P(\kappa_h, t)$. The first method is based on that of Lindborg[10] and results in constant input power. The forcing spectrum, denoted $Q(\kappa_h)$, is Gaussian centered around forcing wave number, κ_f, and with characteristic width, c

$$Q(\kappa_h) = C \exp\left[-\left(\frac{\kappa_h - \kappa_f}{c}\right)^2\right]. \tag{13}$$

The constant C determines the total input power.

The second method for specifying $P(\kappa_h, t)$ is based on that of Overholt and Pope.[22] The resulting spectrum is denoted $R(\kappa_h, t)$. Let $E(\kappa_h, t)$ be the horizontally averaged kinetic energy spectrum of the flow at time t and $E_m(\kappa_h)$ be the target spectrum, that is, the desired $E(\kappa_h, t)$ when the simulation is statistically steady. In a simulation with forcing, the spectrum evolves in time according to

$$\frac{\partial E(\kappa_h, t)}{\partial t} = R(\kappa_h, t) + \Lambda(\kappa_h, t),$$

where $\Lambda(\kappa_h)$ accounts for all of the terms in the Navier-Stokes equations except for forcing. For our horizontally homogeneous isotropic flow scenario, only the horizontal components of velocity with $\kappa_3 = 0$ are forced. Thus,

$$E_f(\kappa_h, t) = \frac{1}{2}\oint(\hat{u}_i(\kappa_1, \kappa_2, 0)\hat{u}_i^*(\kappa_1, \kappa_2, 0))d\mathcal{S}(\kappa_h) \quad \text{for } i = 1, 2 \tag{14}$$

is the part of kinetic energy spectrum directly affected by forcing. The goal is to determine $R(\kappa_h,t)$ as a function of time that will optimally converge $E_f(\kappa_h,t)$ to $E_m(\kappa_h)$. Letting $\mathcal{E}_f(t)$, $R(t)$, and E_m be shorthand notation for $E_f(\kappa_h,t)$, $R(\kappa_h,t)$, and $E_m(\kappa_h)$, respectively, and using dots to indicate differentiation in time,

$$\ddot{E}_f(t) = -\beta\dot{E}_f(t) - \omega_0^2[E_f(t) - E_m] \tag{15}$$

is an ordinary differential equation for a specific value of κ_h with β the damping coefficient and ω_0 the angular frequency at which the solution oscillates. Assuming that the forcing dominates the Navier-Stokes terms until the simulation is nearly converged suggests writing Eq. (15) with $\dot{E}_f(t) = R(t)$. Note that Eq. (15) is critically damped when $\beta = 2\omega_0$. Upon introducing a dimensionless damping factor α, Eq. (15) can be written as

$$\dot{R}(t) = -2\alpha\omega_0 R(t) - \omega_0^2[E_f(t) - E_m]. \tag{16}$$

An under damped, critically damped, and over damped system results when $\alpha < 1$, $\alpha = 1$, and $\alpha > 1$, respectively. The time scale for $R(t)$ to converge to the stationary solution is $\tau = 2\pi/\omega_0$. Letting τ_s be the smallest time scale in the flow then

$$T_f = \frac{\tau}{\tau_s} \tag{17}$$

is the ratio of the response time for the forcing to the response time of the turbulence. Thus, α and T_f are parameters that can be tuned to optimize the convergence characteristics of the simulation.

Equation (16) does not impose any constraint on the sign of R. Recall from Sec. III A that for the force magnitude to be real requires that $P(\kappa_h)$ be non-negative. This requirement is straightforward to enforce in a simulation simply by setting the force to zero, if $R(\kappa_h) < 0$ as is done by Overholt and Pope.[22]

Lastly, it may be desirable to force only some wave numbers, say those below some cutoff value κ_R. In the simulations reported in this paper, setting $R(\kappa_h) = 0$ for $\kappa_h > \kappa_R$ is found to be satisfactory. In other applications, it might be necessary to multiply $R(\kappa_h)$ by a cutoff function such as $\tan h(\kappa_h/\kappa_R)$ (c.f. Ref. 22).

C. Specific forcing schemata

In Secs. III A and III B, the problem of specifying a schema for horizontally homogeneous and isotropic forcing was abstracted into the two problems of prescribing the forcing spectrum, $P(\kappa_h)$ and specifying a force having the desired characteristics and that produces $P(\kappa_h)$. There are endless ways of prescribing the spectrum and specifying the force and so, for specificity, we consider two forces, f and g, and two spectra, Q and R. Of the four possible combinations of force and spectrum schemata, we consider three:

Qf: A constant power schema with force and velocity in phase.

Qg: A constant power schema with force and velocity exactly out of phase.

Rf: A constant energy schema with force and velocity in phase.

All of the schemata force only wave number modes with $\kappa_3 = 0$. As noted by Lindborg,[10] however, it is desirable to excite a small vertical shear when simulating horizontally homogeneous stratified turbulence. To accomplish this, the forcing spectrum is scaled down and a small amount of power is added to the three wave number modes $(0, 0, 3\kappa_m)$, $(0, 0, 4\kappa_m)$, and $(0, 0, 5\kappa_m)$, where κ_m is the smallest nonzero vertical wave number in the simulation. Following Lindborg, 1% of the forcing power is applied to these three modes and the remaining 99% is distributed across the $\kappa_3 = 0$ plane by the forcing schema.

IV. NUMERICAL SIMULATIONS

The characteristics of the three forcing schemata introduced in Sec. III C are studied by implementing them in large eddy simulations. The simulated flow is a solution to the Navier-Stokes equations with the Boussinesq assumption and hyperviscous and hyperdiffusion terms replacing the Stokes viscosity and Fick diffusion terms to represent dynamics at scales smaller than the grid spacing. A force term is included in the momentum equation to implement schemata Qf, Qg, or Rf. The thermal energy equation is written in terms of density, and a mean density gradient, $d\langle\tilde{\rho}\rangle_h/d\tilde{z}$, is imposed, with the tilde over a symbol indicating a dimensional quantity and $\langle\ldots\rangle_h$ denoting the planar mean.

A. Governing equations

The governing equations are written in non-dimensional form in terms of characteristic velocity, length, and density scales, $\tilde{U}$, $\tilde{\ell}$, and $\tilde{\rho}$, respectively. Note that $\tilde{U}$ is a characteristic value, not the specific value from any particular simulation. Similarly, $\tilde{\ell}$ is a characteristic value since, for each of the forcing schemata, the force is applied over a range of length scales. In terms of these scaling parameters, the governing equations are

$$\nabla \cdot \boldsymbol{u} = 0, \tag{18a}$$

$$\frac{\partial \rho}{\partial t} + \boldsymbol{u} \cdot \nabla\rho - w = \frac{1}{\mathrm{Pr}\,\mathrm{Re}_\ell}\nabla^4\rho, \tag{18b}$$

$$\frac{\partial \boldsymbol{u}}{\partial t} + \boldsymbol{u} \cdot \nabla\boldsymbol{u} = -\frac{1}{\mathrm{F}^2}\rho\,\boldsymbol{e}_z - \nabla p + \frac{1}{\mathrm{Re}_\ell}\nabla^4\boldsymbol{u} + \boldsymbol{b}, \tag{18c}$$

TABLE I. Simulation parameters common to all three forcing schemata.

$\ell_h = \tilde{\ell}_h/\tilde{\ell}$	4
$\ell_z = \tilde{\ell}_z/\tilde{\ell}$	0.5
N_h	256 grid points
N_z	32 grid points
F_h	6.17×10^{-2}
Re_l	7.15×10^{12}
Pr	1.0

with the hyperviscous Reynolds, Froude, and turbulent Prandtl numbers defined as

$$\mathrm{Re}_\ell = \frac{\tilde{U}\tilde{\ell}}{\tilde{\nu}_h}, \quad \mathrm{F}_h = \frac{\tilde{U}}{\tilde{N}\tilde{\ell}}, \quad \mathrm{Pr} = \frac{\tilde{\nu}_h}{\tilde{D}_h}.$$

Here, $\tilde{\nu}_h$ is the constant hyperviscosity and $\tilde{D}_h$ is the constant hyperdiffusivity, $\tilde{g}$ is the magnitude of the gravitational acceleration, and $\tilde{N} = \left(-\tilde{g}/\tilde{\rho}_0 \, d\langle\tilde{\rho}\rangle_h/d\tilde{z}\right)^{1/2}$ is the Brunt Väisälä frequency. $\boldsymbol{u} = [u, v, w]$ is the velocity vector, ρ and p are the density and pressure deviations from their hydrostatic values, and $\boldsymbol{e}_z$ is a unit vector in the vertical, z, direction. The pressure has been scaled by the dynamic pressure, $\tilde{\rho}_0 \tilde{U}^2$, and the density by $\tilde{\ell}\left|d\langle\tilde{\rho}\rangle_h/d\tilde{z}\right|$.

A pseudo-spectral technique is used to compute the spatial derivatives and a third-order Adams-Bashforth schema with projection is used to advance the solution in time. A spherical wave-number truncation of approximately $15/16$ κ_{max}, with κ_{max} the maximum wave number in the discrete Fourier transforms, is used to reduce aliasing errors. The momentum equation is advanced in time with the nonlinear term expressed in vorticity form, while the alternating time-step schema suggested by Kerr[31] is employed for the density field to approximate the skew-symmetric form of the nonlinear term and thereby minimize aliasing.[32]

B. Simulation parameters

The simulation parameters can be divided into three groups: those common to all the simulations, those relevant to forcing schemata Qf and Qg, and those relevant to schema Rf. The common parameters, listed in Table I, define the size of the computational domain, the (uniform) grid spacing, and the physical parameters not associated with forcing. In the table, ℓ_h and ℓ_v are the horizontal and vertical dimensions of the three-dimensional computational domain, and N_h and N_v are the corresponding number of grid points. For all the simulations, the velocity fields are initialized to zero everywhere, as is the deviatoric density, ρ.

In the constant power forcing schemata, Qf and Qg, three independent parameters define the forcing. It is convenient to choose these to be the forcing power, $\mathcal{P}$, and the mean, κ_f, and variance, c, of $\mathcal{Q}(\kappa_h)$. The peak value of that function is defined by (c.f. (13))

$$C = \frac{\mathcal{P}}{\int_{\kappa_{min}}^{\kappa_{max}} \exp\left[-\left(\frac{\kappa_h - \kappa_f}{c}\right)^2\right] d\kappa_h},$$

where κ_{min} is the minimum wave number in the discrete Fourier transforms. In terms of the characteristic velocity and length scales, $\mathcal{P} = \tilde{\mathcal{P}}/(\tilde{U}^3/\tilde{\ell})$ and $\kappa_f = 2\pi/\tilde{\ell}$. The parameters for the Qf and Qg simulations are given in Table II. Simulation Qg corresponds exactly to Lindborg's run 1.

TABLE II. Simulation parameters for forcing schema Qf and Qg.

κ_f	4.0
c	3.0
P	1.0

TABLE III. Simulation parameters for forcing schema Rf.

α	1.8
κ_R	10
T_f	0.4

The parameters specific to forcing schema Rf are the target energy spectrum $E_m(\kappa_h)$, the highest wave number forced, κ_R, the damping coefficient, α, and the forcing time scale ratio, T_f. $E_m(\kappa_h)$ is set equal to the stationary solution from case Qf so that the characteristics of the different forcing schemata can be easily compared. The remaining parameters are as shown in Table III. These were determined by trial and error. Most interesting is the behavior of the schema for different values of α. Let $\mathcal{E}_f(t)$ be the total horizontal kinetic energy in all the wave numbers being forced and E_m the corresponding target value. The ratio $\mathcal{E}_f(t)/\mathcal{E}_m$ is plotted versus time in Fig. 1. When Eq. (16) is under damped ($\alpha = 0.4$) or critically damped ($\alpha = 1.0$), then there is significant oscillation of the energy about the target value. When Eq. (16) is over damped ($\alpha = 1.8$), then the energy converges to the target nearly optimally. This result is consistent with those of Overholt and Pope. Of course, convergence of $\mathcal{E}_f(t)/\mathcal{E}_m$ to unity does not ensure convergence of the spectrum to the target spectrum at each wave number, but this was the case in our simulations.

C. Verification

Analysis of the simulation results is divided into three sections. First, it is verified that the prescribed input power

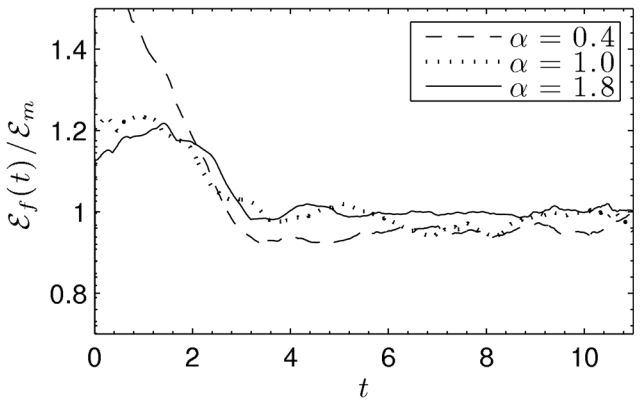

FIG. 1. Time evolution of the ratio of horizontal contribution to kinetic energy at the forcing plane to target energy for schema Rf.

for the Q schemata and the prescribed model spectrum for the R schema are achieved. Second, the performance of the schemata is evaluated in terms of the time it takes for the solution to converge and the overshoot in kinetic energy. Third, some characteristics of schemata are examined in terms of the physical phenomenon that they are designed to emulate.

The most important characteristic of a forcing schema is that the numerical implementation applies the desired force. This may seem like a matter of accurately writing the software, but in light of the insight by Alvelius that the discretized transport equations allow for power inputs that have no analog in the continuous equations, it is worthwhile to verify that the careful theoretical development in Sec. III does indeed carry over to the actual simulations. This has been done for the simulations by verifying that the power input by force-force and force-velocity correlations is as prescribed, that the desired forcing or target spectra result, and that the statistics of the steady-state solutions are independent of the size of the time step in the simulations.

In this paper, demonstration of the numerical implementations is limited to showing that the prescribed power or prescribed model spectrum is achieved. These are shown in Figs. 2(a) and 2(b). In the top panel of the figure, it is evident that the time-averaged forcing spectrum, $\bar{P}(\kappa_h)$, matches that specified by Eq. (13). The over bar denotes time averaging over a period of about one large eddy turn over time, that is, over unity dimensionless time. Also included in the plot is the spectrum of the input power in the Rf schema.

Fig. 2(b) shows the agreement between the target spectrum, E_m, and the steady-state spectrum for schema Rf. As with the Q schemata, the implementation yields the desired results. Also shown in the figure are the steady state spectra for the Q schemata. Recall that the model spectrum was chosen to be the converged spectrum from schema Qf. The spectrum for the Qg schema should not necessarily agree with the other two. From Figs. 2(a) and 2(b) and other analyses not shown, it is concluded that the theory from Sec. III is accurately implemented in the time- and space-discrete simulations.

A principle difference between the f and g forces is expected in their temporal autocorrelations. Let the autocorrelation of the force, $\boldsymbol{b}$, be denoted $\langle \boldsymbol{b} \star \boldsymbol{b} \rangle$ (τ) with τ the separation in time and $\langle\rangle$ indicating that the correlations have been averaged over space. This quantity is plotted for the three forcing schemata in Fig. 3. As expected from the derivation by Alvelius,[30] the g force is not correlated in time and so the autocorrelation is non-zero only at $\tau = 0$. The f force is correlated over a separation time of $\tau > 1$. This is consistent with the idea that the f force represents the effects of coherent structures larger than the simulation domain. The correlation time of the f force as implemented in the Rf schema is slightly less than as in the Qf schemata. This is as expected since the magnitude of the force varies in time with the Rf approach but not with the Qf approach.

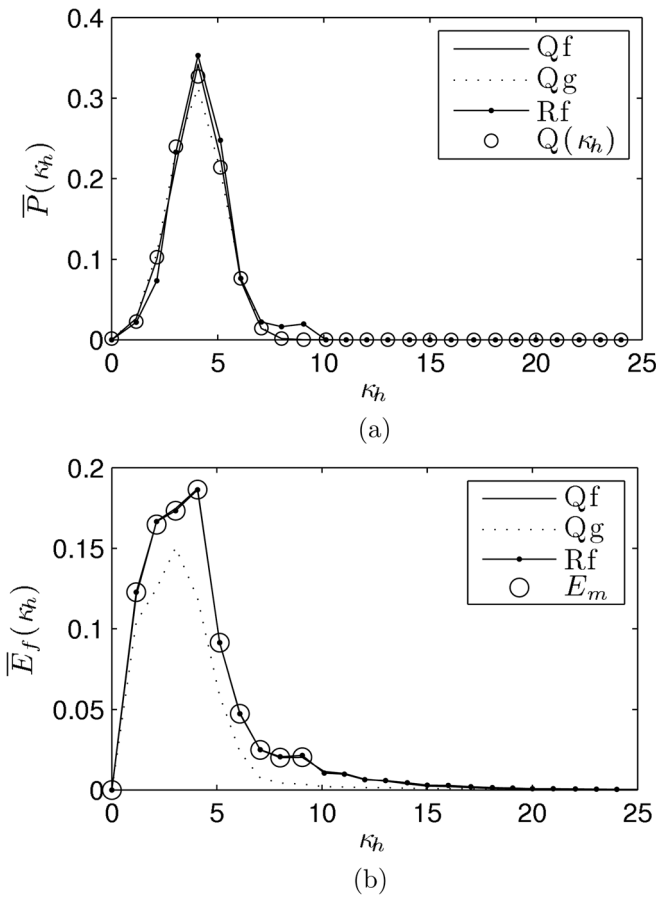

FIG. 2. (a) The agreement between forcing spectrum defined by Eq. (13) and actual injected forcing spectrum for the Qf and Qg schemata. (b) The agreement between model spectrum, $E_m(\kappa_h)$ and $\bar{E}_f(\kappa_h)$ for the Rf schema.

D. Performance

An important metric by which to judge the performance of a forcing schema is the time it takes for the simulation to converge to steady state. Of course, the statistics that must be converged and the criteria by which convergence is judged are dependent on the purpose of the particular simulation. Here, several flow statistics are considered as functions of time in order to gain an appreciation for the convergence characteristics of the three forcing schemata.

1. Dissipation rate and forcing power

Given the choice made in Sec. IV B to make the domain-averaged forcing power a simulation parameter, a

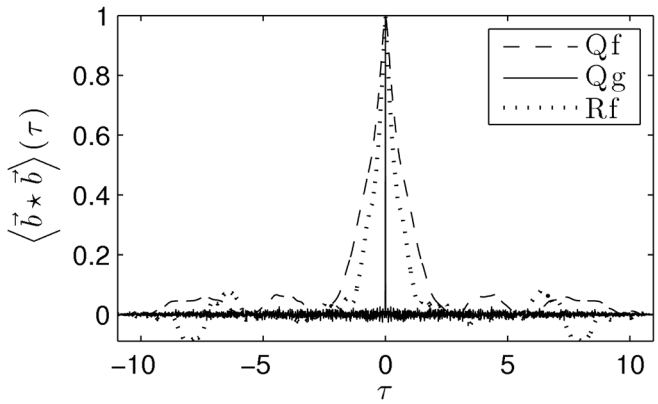

FIG. 3. The spatially averaged temporal autocorrelation of the force, $\boldsymbol{b}$ for each forcing schema.

natural test for convergence is that the total energy dissipation rate, that is, the sum of the dissipation rates of kinetic and available potential energy, equals the forcing power when averaged over time. The total dissipation rate is denoted $\varepsilon(t)$ and is plotted, along with forcing power in Fig. 4. The possibility of time dependent forcing power, as occurs in the Rf schema, is made explicit with the notation $\mathcal{P}(t)$ even though it is, by definition, constant in the Q schemata.

In all cases, $\epsilon(t)$ and $\mathcal{P}(t)$ converge, to the extent that they ever will, by about $t=2$. This transient is a reflection on the flow physics as much as on the forcing schemata as it takes some time for the gradients responsible for dissipation to develop. It is known that this flow transfers energy down scale,[10] and the cascade takes time to develop.

The oscillation of $\epsilon(t)$ about $\mathcal{P}(t)$ in the Q schemata apparently reflects some interaction between the forcing and the flow physics since the Qf and Qg schemata behave differently. Recall that the Qf schema is designed with the thought that the forcing represents the effects of length and time scales larger than those in the simulation domain so that the force is correlated with the velocity. In the Qg schema, the discrete nature of the time-stepping is taken advantage of to add power with the force-velocity correlation zero. The Qg approach has no physical analog but, from Fig. 4, it has the potentially useful characteristic that it produces a more nearly constant dissipation rate than does the Qf schema. With the Rf schema, the dynamics are even more complicated since both $\epsilon(t)$ and $\mathcal{P}(t)$ are responding to the flow. Significant variations over time of both $\mathcal{P}(t)$ and $\epsilon(t)$ occur.

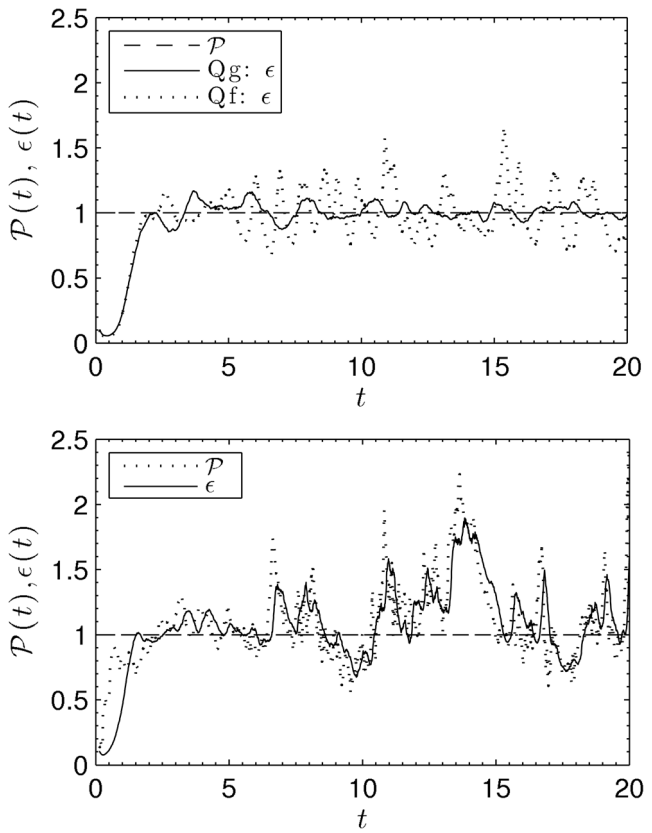

FIG. 4. Time evolution of spatially averaged energy dissipation rate, $\epsilon(t)$ and forcing power, $\mathcal{P}(t)$. The top panel pertains to schemata Qf and Qg, while the bottom panel pertains to schema Rf.

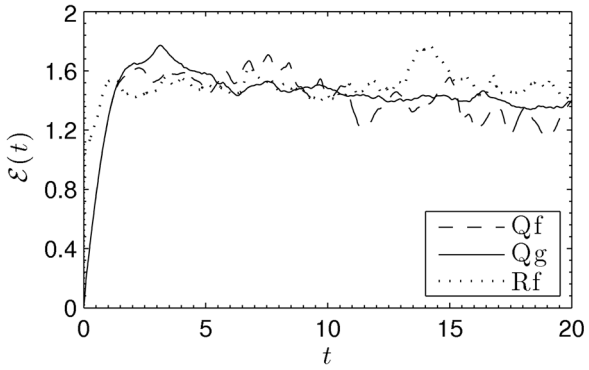

FIG. 5. Time evolution of the domain-averaged kinetic energy, $\mathcal{E}(t)$, for all schemata.

2. Energy

While the time to convergence of the dissipation rate is about the same for all the schemata since it is dependent on the flow physics, the time required for the kinetic energy to converge depends much more strongly on the forcing schema. The domain average kinetic energy, $\mathcal{E}(t)$, is shown for each schema in Fig. 5. Consistent with the results of Lindborg, the Qg schema causes the kinetic energy to overshoot and then converge by about $t=20$. The results of the Qf schema are comparable. The Rf schema, on the other hand, converges the kinetic energy by about $t=2$.

Recall that the force in all the schemata is applied on the plane $\kappa_3=0$, except for the very small forces used to induce vertical shear. The energy on the forced plane, $\mathcal{E}_f(t)$, is shown in Fig. 6. Here it is very evident that the Rf schema converges to the target energy with very little deviation from the time-averaged value after about $t=2$. The target spectrum for the Rf schema was taken from the converged solution for the Qf schema and so, as expected, the Qf and Rf schemata converge to the same energy on the forced plane.

As discussed at the beginning of Sec. II, schemata that emulate physical forces are attractive since the simulation results can then be matched to laboratory flows. For the forcing methods presented in this paper, the characteristics of the forces must be deduced from their effects on the simulated flow. Looking again at Figs. 5 and 6, it is apparent that the Qf and Qg schemata result in comparable time-averaged values of $\mathcal{E}(t)$ yet different values of $\mathcal{E}_f(t)$. Evidently, the

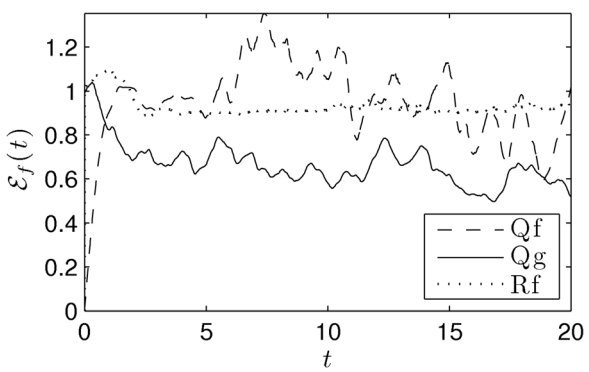

FIG. 6. Time evolution of kinetic energy in the modes being forced, $\mathcal{E}_f(t)$, for all schemata.

average $\mathcal{E}(t)$ is dominated by the flow physics and so it not strongly dependent on the details of the forcing, while the average $\mathcal{E}_f(t)$ does depend on the exact characteristics of the force.

V. APPLICATION TO LABORATORY EXPERIMENTS

It is most straightforward to apply the theoretical concepts from Sec. III to numerical simulations in Fourier space, as discussed in Sec. IV. In laboratory experiments, and in simulations that are not amendable to configuration in Fourier space, it is not as easy to precisely control all aspects of the forces. Nevertheless, the framework for developing forcing schemata is applicable, as are the concepts of forces that are correlated or uncorrelated with the velocity field, stochastic versus deterministic forcing sequences, and power inputs that are constant or variable in time.

To see the relationship between the theory of Sec. III and laboratory experiments, consider, for example, the studies by Variano *et al.*[7,12] of turbulence in a jet-stirred tank. The bottom of the tank is fitted with a planar array of jets that fire water upward toward an air-water interface. The researchers chose the jet spacing, jet diameter, and flow rate, which determine the forcing spectrum. They also chose the duration for which each jet is fired. If the jets are fired for a time that is long compared with the turbulence time scale then a force comparable to our *f* force results, that is, a force that is well-correlated with the velocity. If the duration of each jet pulse is short, then a force analogous to our *g* force is produced. Additionally, the authors note that the firing sequence is randomized to prevent secondary flows just as randomization is used in simulations to break up flow patterns that result in the energy becoming unbounded when forcing is done via linear amplification.

An analogy between the *f* and *g* forces in the forcing framework and real-space counterparts is not perfect. In particular, the *g* force is, by design, an artifact of discrete time in the simulations. It is useful in because it is not correlated with itself in time. In laboratory experiments, a comparable result can be achieved by randomizing the time phase and amplitude of a set of forces with the constraint that the input power is constant. Consider the experiments of Hwang and Eaton[6] and Goepfert *et al.*[8] in which speakers are used to force six jets of air toward the center of a turbulence chamber. Hwang and Eaton[6] randomize the phase and amplitude of the sinusoidal signals sent to the speakers in order to prevent secondary flows with the added effect of reducing the temporal autocorrelation of the force. To achieve a similar effect in simulations, a *g*-type force can be applied. With an unconfined turbulence chamber, Goepfert *et al.*[8] find that randomization of the input to the speakers is not necessary and, as a result, apply a force that has characteristics of our *f* force. The analyses of Sec. III, while seemingly removed from the practical problems of constructing a laboratory experiment, show how decisions that go into the design of an experiment, such as randomizing the force to reduce secondary flows, affect the overall forcing schema.

An important component of the forcing framework is the prescription of the forcing spectrum. Typically, in laboratory experiments, the input power is analogous to our Q spectrum. For example, it is distributed over a limited range of wave numbers determined by the jet configuration in the experiments cited above or the size and spacing of the bars in experiments involving oscillating grids.[5,11] While the input power to the experimental apparatus may be constant, power is only applied to the turbulence by the component of the force aligned with the velocity. The theory in Sec. III suggests that the power transmission will be more effective when a persistent, rather than random, force is applied. Once a forcing pattern is chosen, the power input is adjusted to achieve the desired level of turbulence and changing the pattern, even with the same input power, can be expected to change the turbulence level that results. Goepfert *et al.*[8] describe how the power applied to each of six speakers must be set individually in order to achieve isotropic turbulence because of slight difference in the response of each speaker to the same electrical input. Manual tuning is a form of active feedback, albeit with a very slow feedback loop. Forcing more nearly analogous to our R schema would require active control of the turbulence, which is an area of research in itself.

VI. CONCLUSIONS

As numerical simulation techniques have improved and computers have become more powerful, information from simulations has increasingly been viewed as complimentary to laboratory data. Many researchers envision simulations and laboratory experiments of the same canonical flow to be extremely valuable, with the experiments proving realizability and the simulations providing a detailed description of the flow. A promising approach to developing simulations and experiments of the same turbulent flow is to force the flow to be statistically stationary. The evolution of forcing techniques for both simulations and experiments, however, has relied heavily on trial and error. As a result, the metrics for judging a forcing technique are quite subjective as reflected in the literature reviewed in Sec. II.

In this paper, we take advantage of several decades of work on forcing schemata for isotropic homogeneous turbulence to develop a framework for writing general schemata for applying forces. In this framework, the tasks of choosing the forcing spectrum and choosing the characteristics of the forces are abstracted and treated separately. We then use the framework to write several forcing schemata for horizontally homogeneous and isotropic, vertically stratified flows.

Three forcing schemata, developed in terms of the new framework, are tested in large-eddy simulations. Each has different characteristics and which is "best" depends on the metrics of interest. A deterministic schema with the force and velocity correlated, schema Rf, converges the fastest but the variability in the domain-averaged kinetic energy when the flow is statistically steady is greater than in the other schemata. It also requires a target spectrum to be known *a priori*, which might not be possible. The least variability in kinetic energy at steady state is observed with schema Qg in which the force is uncorrelated with itself in time. It is our bias that the forcing schema should represent motions at

length and time scales that are large compared with those in the simulation. Schema Qg is undesirable on this basis, but the resulting low variance in the domain-averaged kinetic energy is attractive.

The forcing framework applies not just to simulations but to laboratory experiments as well. In experiments, the power input and the length scales at which it is added must be selected. This corresponds to selecting the forcing spectrum and can be controlled in time to achieve a prescribed flow. The forces that add the power can be persistent in time, similar to the *f* forces in the framework, or completely decorrelated in time, as the *g* forces are. It is hypothesized that the effects of the *f* and *g* forces summarized in the preceding paragraph will occur in laboratory experiments with analogous forces.

The simulation results demonstrate the obvious, but important, result that the parameters of a forcing mechanism are highly interrelated. As a consequence, the utility of a particular forcing technique is closely coupled with the purpose of the numerical or laboratory experiment. Using the framework presented in the paper to abstract the components of the forcing schema makes it straightforward to develop a family of schemata for a particular application. Simple test runs in simulations reveal the effects of each forcing method on simulated flows and, thereby, reduce the trial-and-error component of developing laboratory experiments in forced turbulence.

ACKNOWLEDGMENTS

This research was funded by the U.S. Office of Naval Research, Grant No. N00014-04-1-0687 N00014-08-1-0236 managed by Dr. R. D. Joslin. Grants of high performance computer time were provided by the Arctic Region Supercomputing Center and the Army Engineer Research and Development Center.

[1]G. Comte-Bellot and S. Corrsin, "Simple Eulerian time correlation of full and narrow-band velocity signals in grid-generated 'isotropic' turbulence," J. Fluid Mech. **48**, 273 (1971).
[2]S. M. de Bruyn Kops and J. J. Riley, "Direct numerical simulation of laboratory experiments in isotropic turbulence," Phys. Fluids **10**(9), 2125 (1998).
[3]H. Wang and W. K. George, "The integral scale in homogeneous isotropic turbulence," J. Fluid Mech. **459**, 429 (2002).
[4]J. O. Hinze, *Turbulence*, 2nd ed. (McGraw-Hill, New York, 1975).
[5]I. P. D. De Silva and H. J. S. Fernando, "Oscillating grids as a source of nearly isotropic turbulence," Phys. Fluids **6**, 2455 (1994).
[6]W. Hwang and J. K. Eaton, "Creating homogeneous and isotropic turbulence without a mean flow," Exp. Fluids **36**, 444 (2004).
[7]E. A. Variano, E. Bodenschatz, and E. A. Cowen, "A random synthetic jet array driven turbulence tank," Exp. Fluids **37**, 613 (2004).
[8]C. Goepfert, J. L. Marié, D. Chareyron, and M. Lance, "Characterization of a system generating a homogeneous isotropic turbulence field by free synthetic jets," Exp. Fluids **48**, 809 (2010).
[9]J. J. Riley and S. M. de Bruyn Kops, "Dynamics of turbulence strongly influenced by buoyancy," Phys. Fluids **15**(7), 2047 (2003).
[10]E. Lindborg, "The energy cascade in a strongly stratified fluid," J. Fluid Mech. **550**, 207 (2006).
[11]S. S. Shy, C. Y. Tang, and S. Y. Fann, "A nearly isotropic turbulence generated by a pair of vibrating grids," Exp. Thermal Fluid Sci. **14**, 251 (1997).
[12]E. A. Variano and E. A. Cowen, "A random-jet-stirred turbulence tank," J. Fluid Mech. **604**, 1 (2008).
[13]T. S. Lundgren, "Linearly forced isotropic turbulence," in *Annual Research Briefs 2003* (Center for turbulence research, Stanford University Stanford, CA, 2003), pp. 461–473.
[14]C. Rosales and C. Meneveau, "Linear forcing in numerical simulations of isotropic turbulence: Physical space implementations and convergence properties," Phys. Fluids **17**(9), 17 (2005).
[15]A. K. Kuczaj and B. J. Geurts, "Mixing in manipulated turbulence," J. Turbul. **7**, 1 (2006).
[16]E. D. Siggia and G. S. Patterson, "Intermittency effects in a numerical-simulation of stationary 3-dimensional turbulence," J. Fluid Mech. **86**, 567 1978.
[17]J. R. Chasnov, "Simulation of the Kolmogorov inertial subrange using an improved subgrid model," Phys. Fluids A **3**, 188 (1991).
[18]A. Vincent and M. Meneguzzi, "The spatial structure and statistical properties of homogeneous turbulence," J. Fluid Mech. **225**, 1 (1991).
[19]N. P. Sullivan, S. Mahalingam, and R. M. Kerr, "Deterministic forcing of homogeneous, isotropic turbulence," Phys. Fluids **6**(4), 1612 (1994).
[20]S. Grossmann and D. Lohse, "Scaling in hard turbulent Rayleigh-Benard Flow," Phys. Rev. A **46**, 903 (1992).
[21]L. Machiels, "Predictability of small-scale motion in isotropic fluid turbulence," Phys. Rev. Lett. **79**, 3411 (1997).
[22]M. R. Overholt and S. B. Pope, "A deterministic forcing scheme for direct numerical simulations of turbulence," Comput. Fluids **27**, 11 (1998).
[23]R. M. Kerr, "Theoretical investigation of a passive scalar such as temperature in isotropic turbulence," Ph.D. thesis (Cornell University, 1981).
[24]V. Eswaran and S. B. Pope, "Direct numerical simulations of the turbulent mixing of a passive scalar," Phys. Fluids **31**, 506 (1988).
[25]S. Ghosal, T. S. Lund, P. Moin, and K. Akselvoll, "A dynamic localization model for large-eddy simulation of turbulent flows," J. Fluid Mech. **286**, 229 (1995).
[26]D. Carati, S. Ghosal, and P. Moin, "On the representation of backscatter in dynamic localization models," Phys. Fluids **7**(3), 606 (1995).
[27]A. Misra and D. I. Pullin, "A vortex-based subgrid stress model for large-eddy simulation," Phys. Fluids **9**, 2443 (1997).
[28]X. Chen and S. Shan, "High-resolution turbulent simulations using the Connection Machine-2," Comput. Phys. **6**, 643 (1992).
[29]L. P. Wang, S. Y. Chen, J. G. Brasseur, and J. C. Wyngaard, "Examination of hypotheses in the Kolmogorov refined turbulence theory through high-resolution simulations. Part 1. Velocity field," J. Fluid Mech. **309**, 113 (1996).
[30]K. Alvelius, "Random forcing of three-dimensional homogeneous turbulence," Phys. Fluids **11**, 1880 (1999).
[31]R. M. Kerr, "Higher-order derivative correlations and the alignment of small-scale structures in isotropic turbulence," J. Fluid Mech. **153**(31), 31 (1985).
[32]J. P. Boyd, *Chebyshev and Fourier Spectral Methods* (Dover, Mineola, NY, 2001).